Structural imperfections and attendant localized/itinerant ferromagnetism in ZnO nanoparticles

2014 J. Phys. D: Appl. Phys. 47 345003

(http://iopscience.iop.org/0022-3727/47/34/345003)

IOP Publishing Journal of Physics D: Applied Physics
J. Phys. D: Appl. Phys. **47** (2014) 345003 (7pp) doi:10.1088/0022-3727/47/34/345003

Structural imperfections and attendant localized/itinerant ferromagnetism in ZnO nanoparticles

Chao-Yao Yang[1], Yi-Hsuan Lu[1], Wei-Hao Lin[1], Min-Han Lee[2], Yung-Jung Hsu[1] and Yuan-Chieh Tseng[1]

[1] Department of Materials Science and Engineering, National Chiao Tung University, 1001 Ta Hsueh Road, Hsinchu, 30010, Taiwan, Republic of China
[2] Undergraduate Honors Program of Nano Science and Engineering, National Chiao Tung University, 1001 Ta Hsueh Road, Hsinchu, 30010, Taiwan, Republic of China

E-mail: yctseng21@mail.nctu.edu.tw (Y-C Tseng)

Received 6 May 2014, revised 26 June 2014
Accepted for publication 7 July 2014
Published 1 August 2014

Abstract

Using synchrotron-based x-ray magnetic spectroscopy, we report a study focusing on the local symmetry of Cu-dopant and resultant structural imperfections in mediating Cu-doped ZnO nanoparticles' ferromagnetism (FM). Prepared by an antisolvent method, Cu appeared to preferably populate on the basal plane of ZnO with a local symmetry of [CuO_4]. This unique symmetry was antiferromagnetic in nature, while electronically and structurally coupled to surrounded oxygen vacancies (V_o) that yielded a localized FM, because of a strong dependency on the number/location of the [CuO_4] symmetry. Surprisingly, the FM of undoped but oxygen-deficient ZnO appeared to be more itinerant and long-range, where V_o percolated the FM effectively and isotropically through oxygen's delocalized orbital. By adopting the approach of structural imperfection, this study clearly identifies V_o's (defect's) true characters in mediating the FM of magnetic semiconductors which has been thought of as a long-standing debate, and thus provides a different thinking about the traditional extrinsic ferromagnetic-tuning in the semiconductors. It even illuminates recent research concerning the intrinsic FM of low-dimensional systems that contain defects but non-magnetic elements.

Keywords: XMCD, ZnO, defect

(Some figures may appear in colour only in the online journal)

S Online supplementary data available from stacks.iop.org/JPhysD/47/345003/mmedia

1. Introduction

In recent years, defect-induced intrinsic ferromagnetism (FM) in materials has become an emergent field. This phenomenon is particularly notable in low-dimensional systems, such as layered materials of grapheme [1] or MoS_2 [2, 3] that feature tremendous broken symmetries. As structural imperfection is thought of as an intrinsic property of most materials, how the FM emerges as a result of the introduction of structural imperfections is an important and fundamental question, if size-reduction in materials is a continual demand in related technologies. The earliest notice of this phenomenon traces back to the field of dilute magnetic semiconductors (DMS). The discovery of DMS opens up a great opportunity to exploit both the intrinsic spin of the electron and its associated magnetic moment in solid-state devices. Early study of the DMS concerned the uniformity of dopant incorporation, and whether such extrinsic tuning brings intrinsic room temperature ferromagnetism (RTFM) to the semiconductor host [4–6]. In recent years the focus has turned to the specific role played by the defect (oxygen vacancy, V_o) in the attendant phenomena [7–11]. The exact role of V_o remains elusive to date, because it was mostly investigated in the presence of dopant, thus it was hard to isolate its contributions to the RTFM. Moreover, the *prerequisite* of a perfect substitution of dopant for cation in DMS may have imperceptibly set a limited measure for our explorations of V_o. In this study we drive

the research from the perspective of structural imperfection to revisit V_o (defect)'s role, and we find that this approach offers more insights into the subject of debate. Through a unique synthetic route we were able to create a localized, $[CuO_4]$ planar symmetry within the Cu-doped ZnO nanoparticles. Such symmetry was antiferromagnetic (AFM) in nature, while it developed a localized ferromagnetic exchange pathway by coupling to V_o nearby, irrespective of its form of imperfection. Yet for the undoped but V_o-abundant ZnO, V_o surprisingly adopted an itinerant way to spin-polarize ZnO's conduction band, forming a longer range RTFM compared to the former case. Comparison of the above two counterparts helps identify V_o's (namely, defect's) true characters in mediating the RTFM of DMS. This fundamental understanding on one hand may stimulate us to rethink the traditional method of extrinsic ferromagnetic tuning in the semiconductors. On the other hand it may provide a playground for the development of spintronic devices based on low-dimensional systems with similar phenomena.

2. Experiment

Cu-doped ZnO nanoparticles, with an average size of 200 nm in diameter, were prepared by an antisolvent method [12]. An ionic liquid (denoted UCC) was first prepared by mixing urea with choline chloride at a 2:1 molar ratio. An amount of 0.36 g of ZnO powders was then added to 150 g of UCC to give a solution containing 2400 ppm of ZnO. Copper nitrite with a given concentration was dissolved in a mixed solution of ethylene glycol and deionized water (in equal volume), which was used as the antisolvent for ZnO. All the chemicals including urea (Riedel-de Haën, 99.5%), choline chloride (Sigma-Aldrich, 98%), ZnO powders (Sigma-Aldrich, 99%), ethylene glycol (Sigma-Aldrich, 99.8%) and copper nitrate (Sigma-Aldrich, 99%) were used as received. For copper nitrate, the content of other metal ion traces (such as Co, Fe, Ni) is below 0.005%, which can significantly abate their contamination in the doped samples. For the preparation of Cu-doped ZnO nanoparticles, 5 ml of ZnO-containing DES was injected into 160 ml of antisolvent in 5 s in a water bath maintained at 70 °C, followed by a vigorous stirring for 30 min. The resultant white suspending solid (Cu-doped ZnO nanoparticles) was collected by centrifugation and washed with deionized water and ethanol to remove the remaining UCC and impurities. Samples with $x = 0.02$, 0.04 and 0.08, were mainly investigated in this work. To correlate the origin of the RTFM and V_o, oxygen-deficient and oxygen-abundant ZnO (defined as od-ZnO and oa-ZnO henceforth) samples were also prepared, and their states of oxygen deficiency/abundance were confirmed by photoluminescence (PL) spectra. The as-prepared ZnO nanoparticles from the antisolvent process naturally had a great deal of oxygen vacancy, which was referred to the od-ZnO. Effective removal of the oxygen vacancies could be achieved by annealing the od-ZnO powder (0.15 mg) in air at 200 C for 24 h, which produced ZnO with relatively abundant oxygen; namely oa-ZnO. High resolution, synchrotron-based x-ray powder diffraction (XRD) and Rietveld refinements were used to determine crystallographic structures and lattice constants. A transmission electron microscope (TEM) was used to probe the microstructure and atomic-scale images. Magnetic properties (hysteresis) were analysed by a vibrating sample magnetometer (VSM), both at 300 and 50 K. Zn and Cu K-edge extended x-ray absorption fine structure (EXAFS) and x-ray absorption near edge structure (XANES) spectra were collected to reveal the local structures and chemical states of selected atomic species, respectively. X-ray absorption spectra (XAS) and x-ray magnetic circular dichroism (XMCD) were collected over Cu L_2/L_3-, Zn L_3- and O K-edges edges, using a TFY mode fixed to an x-ray incident angle of 30° at room temperature with an x-ray switching polarization of 80%, to provide element-specific, spin-dependent electronic information. All XANES/XMCD data presented in this work have been normalized to corresponding edge-jumps to guarantee a quantitative comparison. All synchrotron experiments were performed at the National Synchrotron Radiation Research Center (NSRRC), Taiwan. All XMCD signals were recorded under a magnetic field of 1 T.

3. Result and discussion

Figure 1(*a*) presents x-dependent XRD patterns and respective Rietveld refinements for the Cu-doped ZnO, where a clear wurtzite hexagonal phase is observed in all samples. Rietveld refinements (figure 1(*b*)), together with an independent, direct calculation from Bragg's law on the (1 0 0) and (0 0 2) diffraction peaks, show that Cu-doping results in an expansion of the basal plane (a_1/a_2-axis) but a shrinkage of the vertical dimension (c-axis). HRTEM image of $x = 0.04$ (figure 1(*c*)), taken from a zone-axis of [2 −1 −1 0] shows a zigzag-like lattice distortion along the basal plane consistent with the XRD results. Both macroscopic (XRD) and microscopic (HRTEM) analyses suggest a structural anisotropic-effect upon Cu incorporation without forming a second phase. Such preferential population of Cu might be related to the inherent property of ZnO nanoparticles [12], in which (0 0 0 1) plane possesses substantially larger surface energy than others and is more prone to being affected by the Cu incorporation.

Figure 2(*a*) compares x-dependent XANES with several reference Cu. The doped Cu appears electronically similar to Cu^{2+} (CuO) with a $3d^9$ configuration, while the vanished pre-edge is indicative of a different local structural symmetry. The pre-edge characteristics can be decomposed into features A and B after differentiation (figure 2(*b*)), which provides a detailed correlation between electronic state and structural symmetry. Feature A corresponds to a quadrupole 1s→3d transition as a characteristic of Cu $3d^9$ state which lacks centro-symmetry in coordination, usually being referred to an atomic substitution of Cu for Zn site with a tetrahedron symmetry [8, 13]. Given that feature A is intrinsically weak in $x = 0.02$ and vanishes in $x = 0.04$ and 0.08, the local symmetry of Cu doesn't appear to be a tetrahedron. Rather, it appears to be a planar $[CuO_4]$ structure as reported by Ma *et al* [8, 13]. (Note that the formula of $[CuO_4]$ here refers to the structural symmetry instead of the valence state.) The Fourier-transformed EXAFS in figure 2(*c*) shows that Cu only contains a single coordination

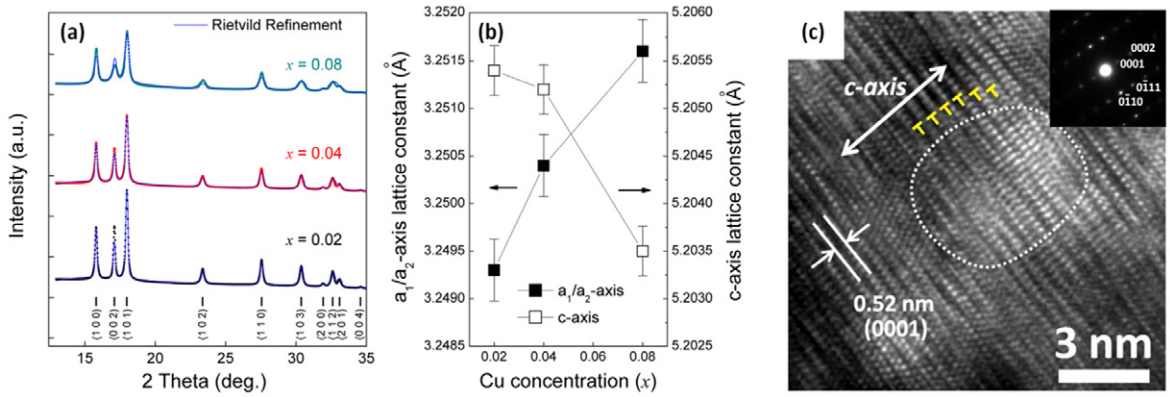

Figure 1. (*a*) XRD patterns and (*b*) lattice constant change (gained from Rietveld refinements (quality of fitting parameters of R_p, R_{wp} and R_{Bragg} all around 5%) and a direct calculation on (1 0 0) and (0 0 2) peaks using Bragg's law, where the error bars were estimated from the deviations between the two means) for the Cu-doped ZnO with x-dependency. (*c*) HRTEM image of $x = 0.04$ sample, where the zigzag-like lattice distortion along the basal direction is highlighted by the dashed circle. Yellow symbols indicate the dislocations arising from the zigzag distortion.

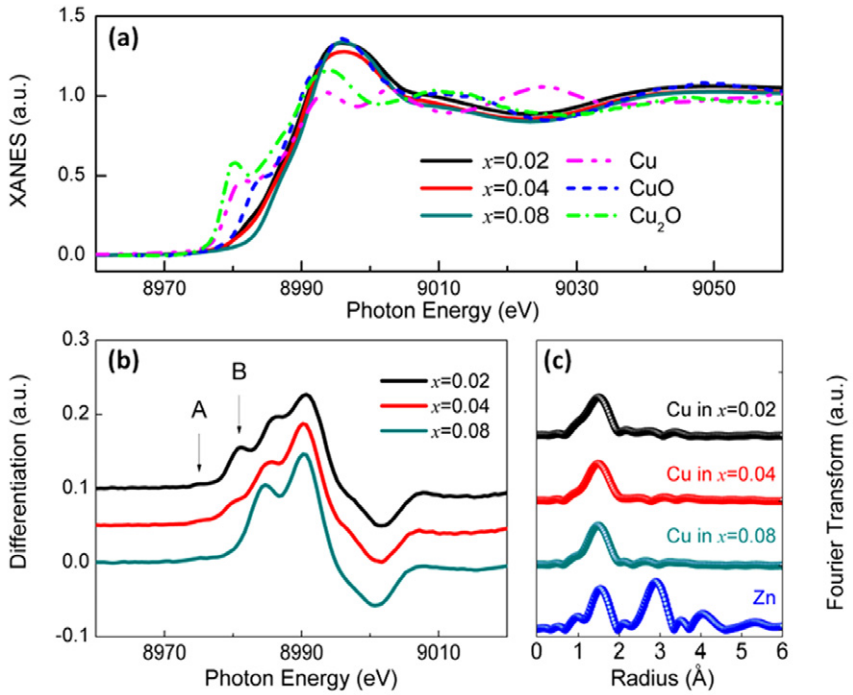

Figure 2. (*a*) Cu K-edge XANES for the Cu-doped ZnO with x-dependency, together with reference samples of Cu, Cu_2O and CuO; (*b*) first derivative of XANES and (*c*) Fourier-transformed EXAFS spectra with x-dependency. A Zn spectrum is given in (*c*) for comparison.

shell in comparison with Zn. This suggests that Cu is locally encompassed by an oxygen environment with a short-range ordering, which resembles the $[CuO_4]$ symmetry. When combining EXAFS with the XRD and TEM information, the symmetry's planar characteristic on the basal plane is validated. Feature B (figure 2(*b*)) is attributed to the $1s \rightarrow 4p$ transition with a final-state screening from 1*s* core hole state, causing a ligand-metal charge transfer (LMCT) as a result of 2p–3d electronic mixing [6, 8, 13]. Feature B is suppressed and shifts towards a lower energy with increasing x because of increased Cu–O covalence. Previous studies [6, 8, 13] found that the Cu–O covalence is increased by shortening the Cu–O bond-length, which often takes place upon the trapping of V_o around Cu, rendering a local coordination modification as $[CuO_y]$ ($y < 4$).

Upon confirmation of the local structure, we turn focus to the attendant magnetic properties. Figures 3(*a*) and (*b*) provide x-dependent magnetic hysteresis (M–H) loops at 300 K and 50 K, respectively. We took data at 50 K rather than lower temperatures considering that Cu-doped ZnO was found to undergo a complex electronic transition for $T < 50$ K [14] that goes beyond the scope of this study. The RTFM is observed for all doped samples, with saturation magnetization (M_s) enhanced progressively with increasing x. It is noteworthy that the Bohr magneton (μ_B) per Cu atom remains unchanged with x, as highlighted in the inset of figure 3(*a*). This phenomenon is fundamentally distinct from the Zn-substituted cases where the moment per TM atom (TM as transition metal) quenches sharply with increasing doping concentration [15–17]. If Zn is atomically substituted, the unoccupied Cu $3d^9$ (Cu^{2+}) state

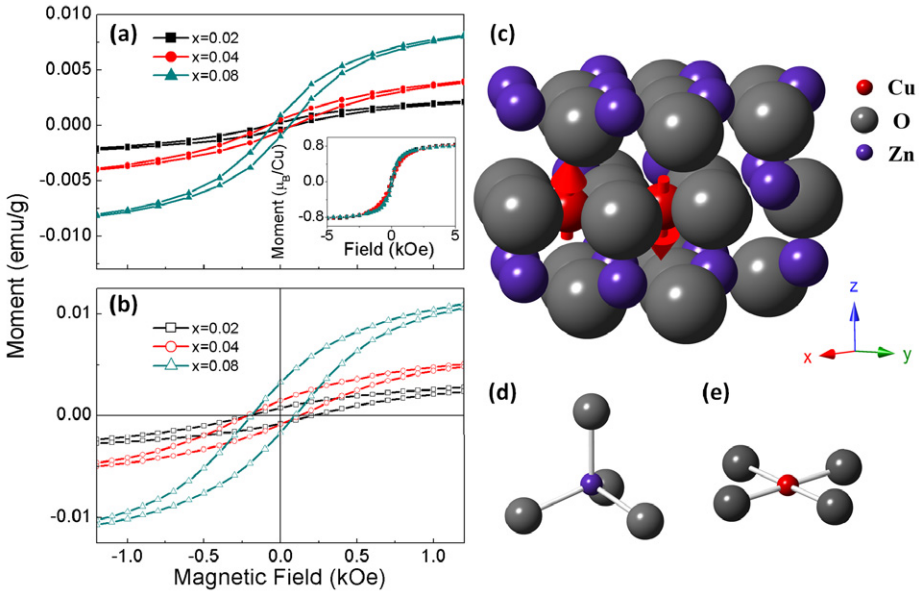

Figure 3. M–H curves of the Cu-doped ZnO with x-dependency collected at (a) 300 K and (b) 50 K. Inset of (a) shows M–H curves after normalizing magnetization to the Cu amount. Inset of (b) is the zoomed-in information for the main panel, which highlights the EB effect. (c) A schematic illustration demonstrates the spin configuration of Cu atom within the ZnO structure; (d) and (e) illustrate the local tetrahedron [ZnO_4] and planar [CuO_4] symmetry, respectively for comparison.

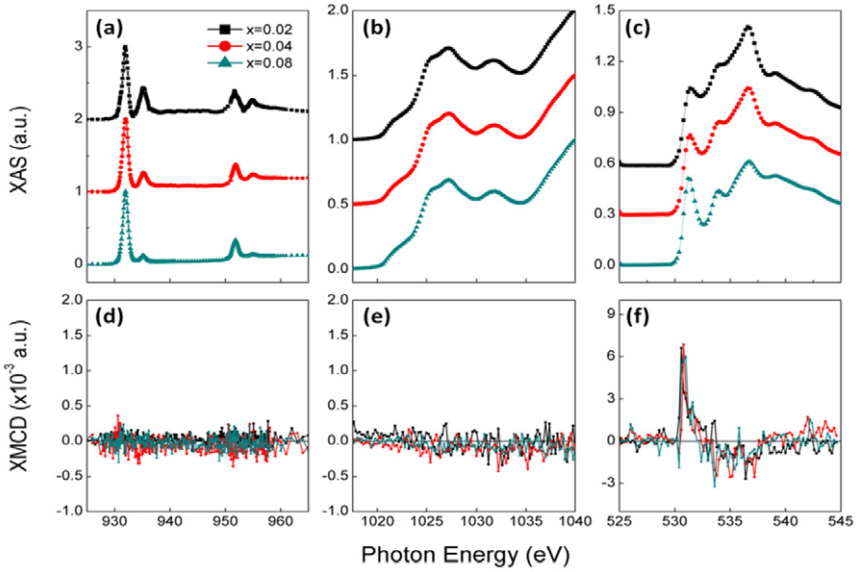

Figure 4. x-dependent XAS spectra for (a) Cu $L_{2,3}$-edge (b) Zn L_3-edge and (c) O K-edge. (d), (e) and (f) are x-dependent XMCD spectra corresponding to (a), (b) and (c), respectively.

is lower than the host conduction state in terms of energy level and, therefore, the electrons of n-type ZnO would tend to occupy the empty Cu $3d^9$ (Cu^{2+}) state leading to a Cu^{1+} state responsible for moment-quenching [18]. Our results point to a different RTFM mechanism arising from the [CuO_4] symmetry in comparison with the Zn-substituted cases. In figure 3(b) we observe an exchange bias (EB) effect accompanying the promoted magnetization of Cu-doped ZnO upon cooling. The EB value reaches ~50 Oe in $x = 0.08$ without field-cooling. Considering that the Cu–O based compounds exhibited an antiferromagnetic (AFM) transition temperature (T_N) of ~231 K [19], the results suggest coexistence of the ferromagnetic and antiferromagnetic (AFM) components in the presence of the [CuO_4] symmetry. Feng *et al* [18] has theoretically predicted that Cu^{2+} would be AFM if a superexchange mechanism is initiated through the Cu–O–Cu path on the basal plane of ZnO, otherwise a ferromagnetic nature should present if the exchange interactions occur along the c-axis [20]. Based on the above information, the crystallography and spin configuration of the [CuO_4] symmetry can be summarized as figure 3(c), along with the illustrations of the tetrahedron [ZnO_4] (figure 3(d)) and planar [CuO_4] (figure 3(e)) symmetries.

Since Cu–Cu is antiferromagnetically coupled, we wonder which element, Zn or O, gives rise to the FM that yields the EB by interacting with the Cu-AFM. Figure 4 presents element-dependent XAS ((a), (b), (c) for Cu, Zn, and O,

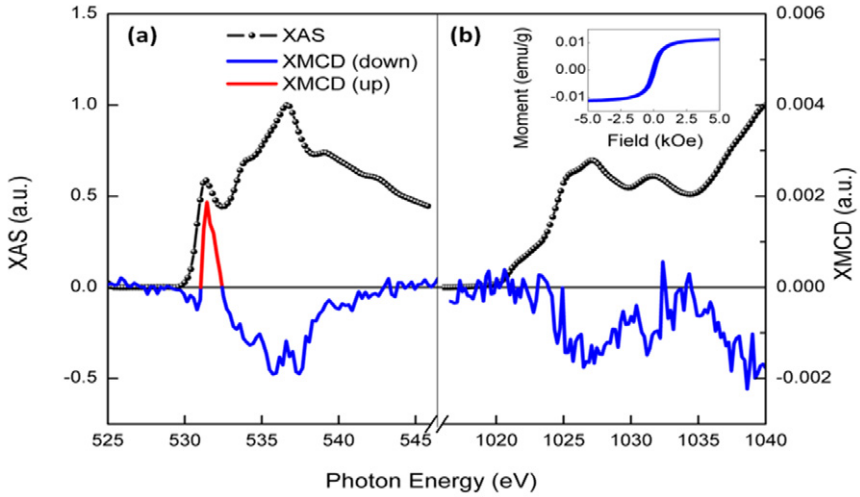

Figure 5. XAS (black) and XMCD (coloured) spectra for (*a*) O K-edge and (*b*) Zn L_3-edge of the od-ZnO. Inset of (*b*) shows the M-H curve of the od-ZnO. The Zn and O XAS share the same units at the left *y*-axis but their XMCD share the same units at right *y*-axis.

respectively) and XMCD ((*d*), (*e*), (*f*) for Cu, Zn, and O, respectively), with *x*-dependency, to elucidate the inter-dependency in electronic/magnetic states among elements. For Cu $L_{2,3}$ XAS (figure 4(*a*)), the major peaks locating at ∼932 eV and ∼952 eV on L_3- and L_2-edge, respectively point to a Cu^{2+} state with a planar coordination [21]. The satellite peaks positioned at ∼935 eV and ∼955 eV refer to a $3d^{10}$ $\underline{L}$ state resulting from the Cu–V_o interaction, where $\underline{L}$ is denoted a hole state on O's valence band [7, 21]. As expected, Cu doesn't contribute XMCD (figure 4(*d*)) due to its AFM nature. Zn's electronic and magnetic states (figures 4(*b*) and (*e*), respectively) appear to be *x*-independent and contribute zero XMCD. XMCD is only detected in O *K*-edge (figure 4(*f*)), which arises from a broad energy range mainly attributed to the dispersive Zn 3d4s/Cu 3d–O 2p hybridization. With increasing *x*, an enhanced pre-edge XAS feature at ∼531 eV is detected (figure 4(*c*)), which is related to a state originating from V_o [21]. The result suggests that the Cu incorporation is accompanied by significant degrees of V_o in the vicinity of the [CuO_4] symmetry. Relating to figure 3(*a*), this also means that the RTFM of Cu-doped ZnO is raised by V_o which is strongly coupled to the [CuO_4] symmetry.

However, we notice that the O XMCD consists of two characteristics, with a sharp part pointing up within a narrow energy range (530–532 eV) but a flat part pointing down over a broad energy range (532–540 eV). Since the direction of XMCD signal sensitively corresponds to the external field direction as well as macroscopic magnetization direction, the signal-asymmetry means that the probed XMCD on O only contributes partially to the RTFM of Cu-doped ZnO. In fact, the signal-asymmetry in O XMCD has been observed in Cu-doped ZnO [7] and defective-TiO_2 [11], but its relation to the macroscopic magnetization is unclear. In terms of electronic structure, the sharp, pointing-up XMCD infers a localized character, while the flat and pointing-down part is more associated with a delocalized nature. To fully understand V_o's role with respect to the RTFM, we investigate the magnetic properties of the od-ZnO sample by presenting its O and Zn XAS/XMCD data in figures 5(*a*) and (*b*), respectively, along

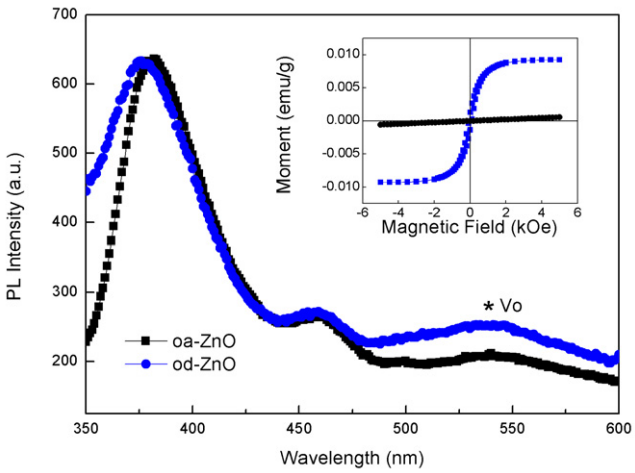

Figure 6. PL spectra of the oa-ZnO (black) and od-ZnO (blue). V_o related luminescence locates at a wavelength of ∼545 nm and it is labelled by a star symbol. The inset shows the *M*–*H* curves of the oa-ZnO (black) and od-ZnO (blue).

with its *M*–*H* loop (measured by a VSM) given in the inset of figure 5(*b*). PL and *M*–*H* data of the od-ZnO/oa-ZnO shown in figure 6 and its inset, respectively, confirm that the RTFM indeed arises from V_o, where the manifested PL signal at ∼545 nm refers to an oxygen-deficient state [22, 23]. Back to figures 5(*a*) and (*b*), both O and Zn display extensive pointing-down XMCD in the od-ZnO and their signal intensities are comparable. These pointing-down XMCD signals apparently arise from a V_o-induced, broad spin-polarized Zn 3d4s–O 2p conduction band. They represent the true magnetic responses to the external field, serving as the real contributors to the od-ZnO's RTFM. Therefore, the pointing-up O XMCD of the od-ZnO (marked by red in figure 5(*a*)) can be understood as an opposite moment against the external field also induced by V_o, which makes no contribution to the RTFM.

With this perspective, however, one would easily argue the origin of the RTFM of Cu-doped ZnO, because XMCD is only detected in O but it is dominated by the one against the external

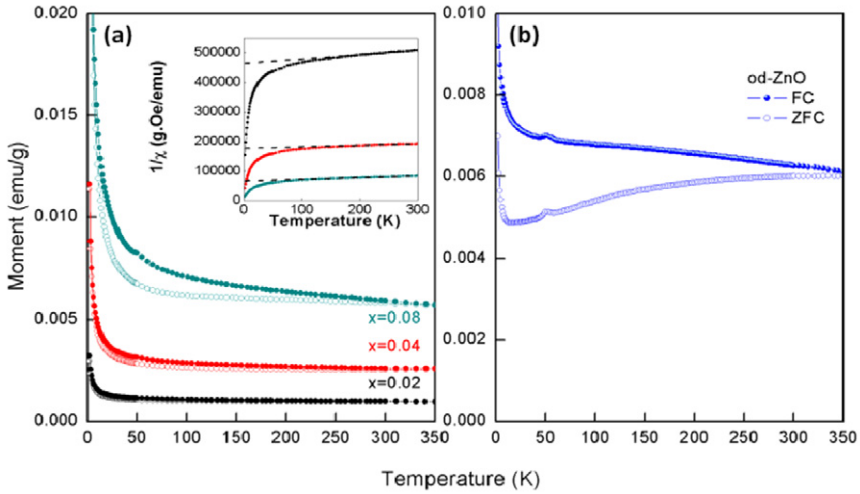

Figure 7. (*a*) Temperature-dependent magnetization (M–T) curves of the Cu-doped ZnO (main panel) with x-dependency taken at field-cooled (FC, closed symbols) and zero-field-cooled (ZFC, open symbols) conditions. Inset shows their $1/\chi - T$ (inversion of susceptibility versus temperature) and the Curie–Weiss fittings (dashed-lines). (*b*) FC and ZFC M–T of the od-ZnO.

field. Similar controversy exists in several Cu-doped ZnO studies also using x-ray absorption spectroscopy: Thakur [21], Keavney [24] and Vachhani [25] *only* found XMCD on Cu but its hysteresis was paramagnetic-like, which contradicted the RTFM they observed macroscopically. Another research study by Herng [7] observed the disappearance of the RTFM by preparing Cu-doped ZnO in an O-rich condition, while given an O-deficient condition the RTFM was restored. These studies together with ours suggest that the true RTFM source may likely locate at V_o rather than at Cu, Zn, or O; however, the long-standing confusion about V_o's role with respect to the RTFM could be attributed to that, as a type of broken symmetry, V_o is unfortunately undetectable by any available technique. V_o's characters, so far in several studies [7, 11, 21], were only partially reflected by the behaviours of the remaining constituent, such as oxygen. We believe that V_o breaks the local symmetry and re-distributes the spins with lattice distortion, performing as a type of Jahn–Teller effect [26]. It provides high spin-polarization with the residence of free spins, in analogy to the intrinsic FM observed in nanostructures featuring large broken symmetry at the surface but containing non-magnetic elements [1–3, 27]. In Cu-doped ZnO, V_o produces the FM through a localized route according to the localized electronic characteristics found in O XAS (figure 4(*c*)) and XMCD (figure 4(*f*)). However, such localized electronic characteristics are electrically and structurally coupled to the [CuO_4] symmetry, as validated by O XAS and XMCD, even if the [CuO_4] is antiferromagnetically coupled itself. This explains why the magnetization enhances with increasing Cu concentration (main panel of figure 3(*a*)) but once normalized to Cu amount the magnetization remains unchanged (inset of figure 3(*a*)), because only those V_o coupled to Cu contribute to the magnetization. Though the pointing-down O XMCD suggests some delocalized magnetic character of Cu-doped ZnO, this effect is secondary compared to the direct magnetization provision from V_o that is tightly bound to Cu. However, a different physical route is adopted by V_o in the od-ZnO where an itinerant FM is regulated directly through O's delocalized orbital. Temperature-dependent magnetization (M–T) data, as given in figure 7, clearly differentiate Cu-doped ZnO and od-ZnO due to different FM behaviours. An upward curvature observed in the M–T of Cu-doped ZnO suggests a Curie–Weiss like behaviour. However, their $1/\chi$–T (inversion of susceptibility versus temperature) display a notable deviation from the Curie–Weiss law at low temperature. This phenomenon is attributable to a short-range FM, or a spin-cluster character within a matrix of spin-disorder [28–30]. On the contrary, the od-ZnO exhibits a downward curvature in M–T. This feature corresponds to a positive exchange coefficient (J_{ex}) commonly seen in transition metals, which indicates a long-range FM [31, 32]. In figure 8 we provide two models to schematically illustrate the localized/itinerant FM of the Cu-doped ZnO /od-ZnO from the viewpoint of crystallography and spin configuration. In figure 8(*a*), both Zn and O display atomic moments when V_o is nearby in the case of od-ZnO, which is supported by the data of figures 5 and 6. For Cu-doped ZnO (figure 8(*b*)), Cu atoms are antiferromagnetically coupled themselves via the [CuO_4] symmetry, and then net moments are only present at the open sites of V_o, according to the data of figures 3 and 4.

4. Conclusions

In summary, we have intensively investigated the contributions of structural imperfections (V_o and [CuO_4]) to the ZnO's intrinsic FM, with a strong attempt to capture the spirit of the field of defect FM that emerges in recent years. The study is informative in several aspects. First, dopant strongly influences the structural and electronic properties of the spintronic systems [4–6, 13, 21], yet it may not necessarily play as a *direct* magnetic contributor, irrespective of its form of perfection (Zn-substituted cases, [21, 24, 25]) or imperfection (our case). Therefore, the traditional extrinsic ferromagnetic-tuning needs to be properly implemented and, even to be reconsidered. In fact, a previous study [33] (Zn-substituted by Co) and ours point to a fact that dopant may easily attract V_o due to structural relaxation, hence limiting the

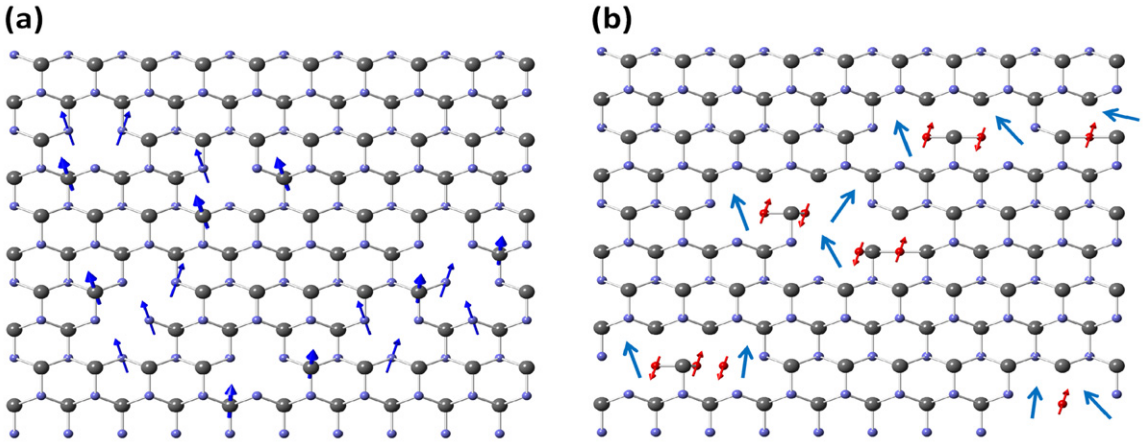

Figure 8. Schematic illustrations for the spin configurations of the (*a*) od-ZnO and (*b*) Cu-doped ZnO. For (*a*), the net moments (deep blue) locate at both Zn (small balls) and O (big balls) as supported by figure 5, while for (*b*) the net moments (light blue) locate at the open sites of V_o with detailed description in the related content. The red arrows in (*b*) represent the antiferromagnetic nature of Cu.

ferromagnetic strength as reported in this study. However, the spins stored by imperfections' sites are rather unbounded; they are free from crystallographic confinement, so they could enable ferromagnetic exchange interactions more isotropically. Of course the level of the exchange interactions would depend on the amount and type of the broken symmetry. This study may illuminate recent research concerning the intrinsic FM of low-dimensional materials [1–3, 27] which contain defects but non-magnetic elements.

Acknowledgments

The authors would like to express appreciation to Professor H Chou for fruitful discussions, and also thank Mr Fan-Hsiu Chang for the XMCD data collection at NSRRC beamline 11 A. This work is supported by the National Science Council of Taiwan and National Chaio Tung University, under Grant Nos NSC 101-2112-M-009 008-MY3 and NCTU-101W9886, respectively.

References

[1] Khurana G, Kumar N, Kotnala R K, Nautiyald T and Katiyar R S 2013 *Nanoscale* **5** 3346
[2] Tongay S, Varnoosfaderani S S, Appleton B R, Wu J and Hebard A F 2012 *Appl. Phys. Lett.* **101** 123105
[3] Zhang Z, Zou X, Crespi V H and Yakobson B I 2013 *ACS Nano* **7** 10475
[4] Sun Z *et al* 2008 *Phys. Rev.* B **77** 245208
[5] Wang X, Xu J B, Cheung W Y, An J and Ke N 2007 *Appl. Phys. Lett.* **90** 212502
[6] Liu H, Zeng F, Gao S, Wang G, Song C and Pan F 2013 *Phys. Chem. Chem. Phys.* **15** 13153
[7] Herng T S *et al* 2010 *Phys. Rev. Lett.* **105** 207201
[8] Ma Q, Prater J T, Sudakar C, Rosenberg R A and Narayan J 2012 *J. Phys.: Condens. Matter.* **24** 306002
[9] Wang Q, Sun Q, Chen G, Kawazoe Y and Jena P 2008 *Phys. Rev.* B **77** 205411
[10] Xu Q, Schmidt H, Zhou S, Potzger K, Helm M, Hochmuth H, Lorenz M, Setzer A, Esquinazi P, Meinecke C and Grundmann M 2008 *Appl. Phys. Lett.* **92** 082508
[11] Thakur H, Thakur P, Kumar R, Brookes N B, Sharma K K, Singh A P, Kumar Y, Gautam S and Chae K H 2011 *Appl. Phys. Lett.* **98** 192512
[12] Dong J-Y, Hsu Y-J, Wong D S-H and Lu S-Y 2010 *J. Phys. Chem.* C **114** 8867
[13] Ma Q, Buchholz D B and Chang R P H 2008 *Phys. Rev.* B **78** 214429
[14] Xing G Z *et al* 2008 *Adv. Mater.* **20** 3521
[15] Lu Z, Hsu H S, Tzeng Y, Zhang F, Du Y and Huang J C 2009 *Appl. Phys. Lett.* **95** 062509
[16] Ramachandran S, Narayan J and Prater J T 2006 *Appl. Phys. Lett.* **88** 242503
[17] Chakraborti D, Narayan J and Prater J T 2007 *Appl. Phys. Lett.* **90** 062504
[18] Feng X 2004 *J. Phys.: Condens. Matter* **16** 4251
[19] Koo H-J and Whangbo M-H 2003 *Inorg. Chem.* **42** 1187
[20] Herng T S, Lau S P, Yu S F, Yang H Y, Ji X H, Chen J S, Yasui N and Inaba H 2006 *J. Appl. Phys.* **99** 086101
[21] Thakur P, Bisogni V, Cezar J C, Brookes N B, Ghiringhelli G, Gautam S, Chae K H, Subramanian M, Jayavel, R and Asokan K 2010 *J. Appl. Phys.* **107** 103915
[22] Cheng Y, Hao W, Xu H, Yu Y X, Wang T, Chen R, Zhang L, Du Y, Wang X L and Dou S X 2012 *ACS Appl. Mater. Interfaces* **4** 4470
[23] Kim Y and Kang S 2010 *J. Phys. Chem.* B **114** 7874
[24] Keavney D J, Buchholz D B, Ma Q and Chang R P 2007 *Appl. Phys. Lett.* **91** 012501
[25] Vachhani P S, Dalba G, Ramamoorthy R K, Rocca F, Sipr O and Bhatnagar A K 2012 *J. Phys.: Condens. Matter* **24** 506001
[26] O'Brien M C M and Chancey C C 1993 *Am. J. Phys.* **61** 688
[27] Carmen Muñoz M, Gallego S and Sanchez N 2011 *J. Phys.: Conf. Ser.* **303** 012001
[28] Cullity B D and Graham C D 2009 *Introduction to Magnetic Materials* (Hoboken, NJ: Wiley) pp 125–7
[29] Wu K, Gu S, Tang K, Ye J, Zhu S, Zhou M, Huang Y, Xu M, Zhang R and Zheng Y 2012 *J. Magn. Magn. Mater.* **324** 1649
[30] Furdyna J K, Samarth N, Frankel R B and Spalek J 1988 *Phys. Rev.* B **37** 3707
[31] Bhatt R N, Wan X, Kennett M P and Berciu M 2002 *Comput. Phys. Commun.* **147** 684
[32] Bolduc M, Awo-Affouda C, Stollenwerk A, Huang M B, Ramos F G, Agnello G and LaBella V P 2005 *Phys. Rev.* B **71** 033302
[33] Ciatto G, Trolio A D, Fonda E, Alippi P, Testa A M and Amore Bonapasta A 2011 *Phys. Rev. Lett.* **107** 127206